ACS Catalysis

pubs.acs.org/acscatalysis Research Article

Single Pd Atom−In_2O_3 Catalyzes Production of CH_3CH_2OH from Atom-Economic C−C Coupling of HCHO and CH_4

Yuntao Zhao, Natalie Fontillas, Hua Wang, Xinli Zhu,* Donghai Mei, and Qingfeng Ge*

Cite This: *ACS Catal.* 2024, 14, 1714−1724 Read Online

ACCESS | Metrics & More | Article Recommendations | Supporting Information

ABSTRACT: Using methane as a reagent to synthesize high-value chemicals and high-energy density fuels through C−C coupling has attracted intense attention in recent decades, as it avoids completely breaking all C−H bonds in CH_4. In the present study, we demonstrated that the coupling of HCHO with the CH_3 species from CH_4 activation to produce ethanol can be accomplished on the single Pd atom−In_2O_3 catalyst based on the results of density functional theory (DFT) calculations. The results show that the supported single Pd atom stabilizes the CH_3 species following the activation of one C−H bond of CH_4, while HCHO adsorbs on the neighboring In site. Facile C−C coupling of HCHO with the methyl species is achieved with an activation barrier of 0.56 eV. We further examined the C−C coupling on other single metal atoms, including Ni, Rh, Pt, and Ag, supported on In_2O_3 by following a similar pathway and found that a balance of the three key steps for ethanol formation, i.e., CH_4 activation, C−C coupling, and ethoxy hydrogenation, was achieved on Pd/In_2O_3. Taking the production of acetaldehyde and ethylene on the Pd/In_2O_3 catalyst into consideration, the DFT-based microkinetic analysis indicates that ethanol is the dominant product on the Pd/In_2O_3 catalyst. The facile C−C coupling between HCHO and dissociated CH_4 makes formaldehyde a potential C1 source in the conversion and utilization of methane through an energy- and atom-efficient process.

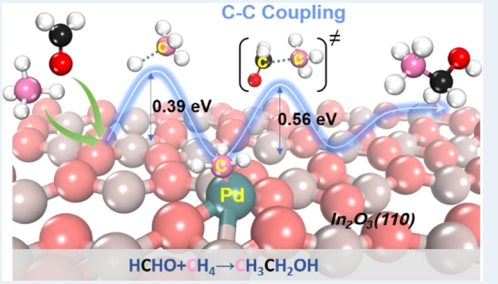

KEYWORDS: *single atom, Pd/In_2O_3, CH_4, HCHO, C−C coupling, ethanol, DFT*

INTRODUCTION

Both CH_4 and CO_2 are greenhouse gases and have been believed to contribute to climate change.[1,2] Reducing CO_2 emissions to eventually achieve carbon neutrality has been recognized as essential to reach the Paris Agreement of limiting global warming to 1.5 or 2 °C.[3] However, CH_4 presents a more severe greenhouse effect than CO_2 and is responsible for at least a quarter of global warming according to the recent literature[4,5] and United Nations reports (26th and 27th Conference of the Parties of United Nations Framework Convention on Climate Change). Furthermore, methane has also an adverse effect on tropospheric ozone and ecosystems.[6,7] Therefore, reducing methane emissions is an urgent challenge.

Converting methane to valuable chemicals other than direct combustion is a promising method for methane optimization and utilization. Since the 1980s, the oxidative coupling of methane catalyzed by metal oxides has been a research emphasis.[8,9] Valuable C_{2+} chemicals can be obtained by coupling the CH_3· radicals produced on the catalyst surface. However, unavoidable overoxidation makes the selectivity of oxidative coupling a longstanding challenge. CH_4 can be used in synthesizing high-energy density chemicals with maximum atom economy when the methyl species from CH_4 activation can be stabilized on the active sites of the catalysts.[10] For example, Pt(II) salts have been reported to catalyze the oxidative conversion of CH_4 to methanol at low temperatures from a Pt-methyl intermediate.[11] Periana et al. employed Pd(II) in the liquid phase to activate the C−H bond of CH_4, generating a Pd-CH_3 species, which could be condensed with methanol to produce acetic acid.[10] In organometallics, the insertion of CO into the Ni-CH_3 σ bond of $[NiCH_3(L)]BPh_4$ to form a C−C bond has been demonstrated.[12,13]

In heterogenous catalysis, the conversion of CH_4 via C−C coupling provides one of the most attractive routes to synthesize long-carbon chain chemicals and fuels. In previous studies, we demonstrated that C−C coupling of the methyl species from CH_4 activation and CO_2 could be realized by following either the Eley−Rideal mechanism or Langmuir−Hinshelwood mechanism.[14,15] Bader charge analysis showed that CO_2 acted as an electrophile, attacking the carbon of the methyl species. If an electrophile stronger than CO_2 reacts with CH_4, the activity of C−C coupling is expected to be higher. Since formaldehyde is a stronger electrophile than CO_2 and widely available, it can be used as a reagent to convert CH_4 to longer carbon chain products. Formaldehyde is also an indoor

Received: October 27, 2023
Revised: December 21, 2023
Accepted: January 3, 2024
Published: January 18, 2024

https://doi.org/10.1021/acscatal.3c05163
ACS Catal. 2024, 14, 1714−1724

volatile organic compound and severely threatens human health.[16,17] To meet the limitation criteria of formaldehyde emission, both adsorption[18−21] and catalytic oxidation[22−25] of formaldehyde to CO_2 have been studied. Converting HCHO with CH_4 could help reduce HCHO emission while also alleviating the CO_2 emission.

Although the C−C coupling of CH_4 with formaldehyde is rarely reported, there have been studies reporting the formation of C−N and C−O bonds using the formaldehyde cation with ammonia and water.[26] Furthermore, formaldehyde serves as an active reactant in aldol condensation with carbonyl reactants to grow the carbon chain.[27,28] Notably, Liu and co-workers reported the collision of the formaldehyde cation with CH_4 and studied the effect of collision energy and vibrational excitation on the reaction.[29] They showed that the H elimination channel, which generates an ethanol-like structure through C−C bond formation, is energetically more favorable than the H abstraction channel, although the H elimination channel accounts for only 15% of the total conversion. Among the four covalent complexes formed through C−C or C−O coupling, the transition state of $CH_3CH_2OH^+$ formation has the lowest energy. Zhang et al. demonstrate that insertion of CO into the Ni-CH_3 bond followed by reduction produces acetaldehyde, which can be further hydrogenated to ethanol,[30] whereas half of the adsorbed CO species were believed to convert to formaldehyde on Ni (111).[31] These studies indicated the possibility of C−C coupling of formaldehyde with activated CH_4 under the heterogenous conditions. Recently, Chang et al. showed that ethanol production from formaldehyde and methane was possible on a dual-function catalyst including a single Fe atom and a frustrated Lewis Pair, with the CH_4 dissociation of an activation barrier of 1.15 eV being the rate-limiting step.[32]

In recent years, single-atom catalysis has become an emerging area in catalysis research.[33,34] For example, the singly dispersed Pd atoms anchored on TiO_2 showed an apparent activation barrier of 28.9 kJ/mol for more than 10 Sonogashira C−C coupling reactions.[35] Herein, we designed a single Pd atom on the In_2O_3 catalyst that enables C−C coupling of formaldehyde and methane by combining the outstanding activity of Pd for both C−H bond activation and C−C coupling reaction[35−37] and the activity of In_2O_3 for concerted C−C coupling reactions.[15]

In the present work, we used the density functional theory (DFT) calculation to study the selective activation of CH_4 on the single Pd site and the adsorption of formaldehyde on the In site. The detailed reaction mechanism for the C−C coupling reaction and the elementary steps leading to the production of ethanol, acetaldehyde, and ethylene were discussed. We also studied the C−C coupling reaction on other single metal atoms supported on the In_2O_3 surface and found a balanced relationship between activation of the C−H bond in CH_4, C−C coupling, and ethoxy hydrogenation steps. DFT calculations together with microkinetic analysis showed that ethanol was the dominant product on the Pd single atom−In_2O_3 catalyst.

METHODS

All spin-polarized calculations were performed using the Vienna Ab initio Simulation Package (VASP).[38,39] The Perdew−Burke−Ernzerhof (PBE) functional was used to determine exchange and correlation energies.[40] The effective cores were described by the projector-augmented wave (PAW) potentials.[41,42] The wave functions of valence electrons were expanded using the plane wave basis set with a cutoff energy of 400 eV. For the In atom, the semicore 5s, 5p, and $4d^{10}$ states were treated explicitly as valence states. For geometry optimization, either the conjugate gradient algorithm or the quasi-Newton scheme was adopted until the forces on the unconstrained atoms were less than 0.03 eV/Å and a (2 × 2 × 1) k-point grid was used to sample the Brillouin zone. Reaction pathway mapping implemented in Materials Studio in combination with the geometry optimization in the VASP code was employed to isolate the transition states. Since the adsorption of the molecular products in this work is nonactivated, no transition states were considered for their desorption.

The body-centered cubic bixbyite In_2O_3 bulk structure with calculated lattice parameters $a = b = c = 10.2302$ Å was used to generate the active low-index surfaces. According to the study of Walsh and Catlow, (110) and (111) surfaces are the two most stable surfaces and the surface energy of the (110) surface (1.070 J/m^2) is slightly higher than that of the (111) surface (0.891 J/m^2).[43] By analyzing the atomic configuration, the (111) surface was found to consist of a stepped In−O chain involved in the (110) surface and, therefore, chose In_2O_3(110) in the present study.

The slab simulating the In_2O_3(110) surface consists of 48 O atoms and 32 In atoms, distributed in four atomic layers, and each layer contains two In−O chains. The vacuum space is 15 Å. For geometry optimization, the bottom two layers were fixed and the top two layers together with the adsorbates on the surface were allowed to relax. The single Pd atom was supported on In_2O_3(110) by connecting with surface In and O atoms. We tested three possible configurations of a single Pd atom on the surface and selected the most stable configuration as the model catalyst, as shown in Figure 1. The single Pd atom

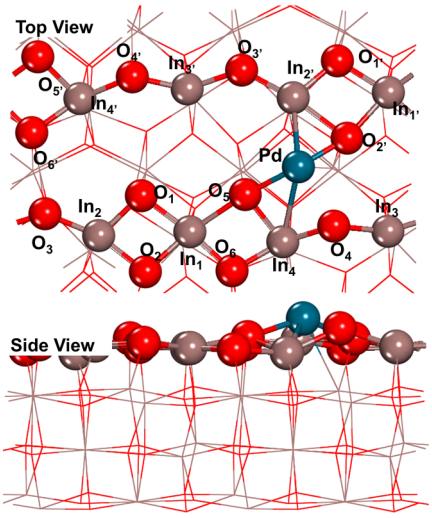

Figure 1. Optimized structure of a single Pd atom supported on In_2O_3(110). In, O, and Pd atoms are colored in brown, red, and blue, respectively. The color scheme was used throughout the work.

was anchored on the surface by linking with two In atoms and forming two Pd−O bonds, with distances of 3.02 2.62, 2.16, and 2.27 Å for Pd−In_4, Pd−$In_{2'}$, Pd−$O_{2'}$, and Pd−O_5, respectively. Other configurations are shown in the Supporting Information. Using the same definition of adsorption energy as that in our previous study,[15] a positive value indicates a thermodynamically favorable process, whereas a negative one

https://doi.org/10.1021/acscatal.3c05163
ACS Catal. 2024, 14, 1714−1724

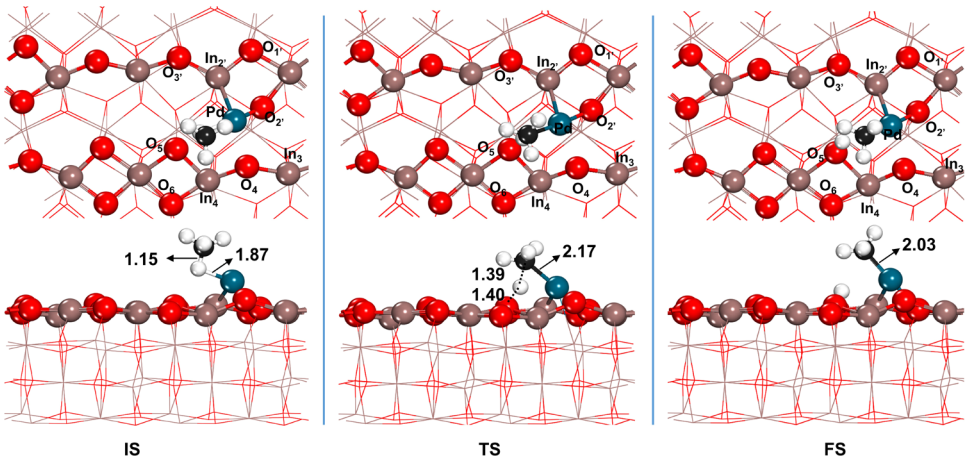

Figure 2. Initial (IS), transition (TS), and final states (FS) of CH_4 dissociation on Pd/In_2O_3(110). Top views are shown in the top row, and the side views in the bottom row. The distances are given in Å. C and H atoms are colored black and white, respectively.

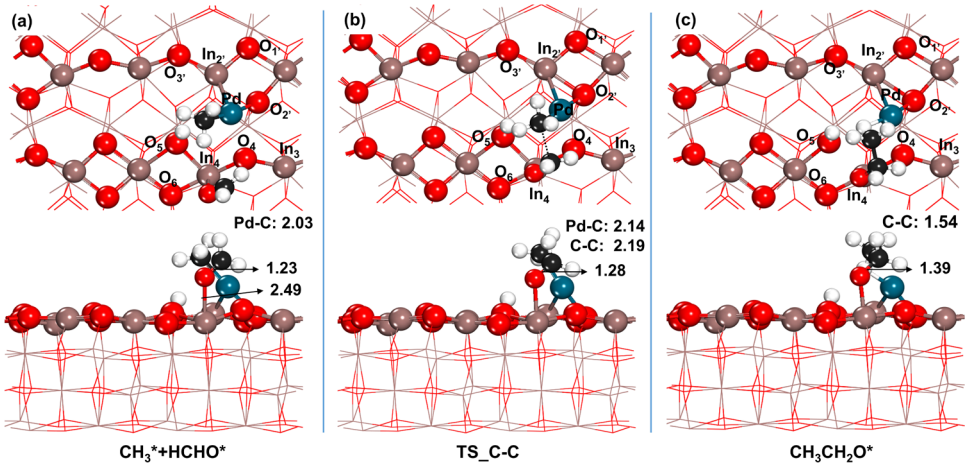

Figure 3. Structures of HCHO adsorption (a) and transition (b) and final (c) states of C−C coupling. Distances are in Å. Top and side views are shown in the upper row and bottom row, respectively.

corresponds to an endothermic adsorption. All optimized structures, including transition states, were confirmed by normal-mode frequency analysis. To analyze the product selectivity on the single-Pd atom−In_2O_3 (110) catalyst, we performed a microkinetic analysis with a mean-field approximation based on the DFT-calculated energetics and the harmonic vibrational frequencies. The details are provided in the Supporting Information.

RESULTS AND DISCUSSION

CH_4 Dissociation on Pd/In_2O_3(110). The Pd active site has been shown to have an enhanced activity for the activation of the C−H bond in CH_4.[36,37] As shown in Figure 1, the single Pd site on the In_2O_3(110) surface was used to activate the C−H bond of CH_4. In our previous study, CH_4 dissociation on both the In−O and O−O pairs was examined, and the results show that the C−H bond activation on the In−O pair has an activation barrier of 1.57 eV and the activation barrier on the O−O pair, with the value of 1.86 eV, is even higher.[15] Therefore, we considered only the Pd−O pair as the active site for C−H bond activation in the present study. The structures of CH_4 adsorption as well as the transition and final states of C−H bond activation are shown in Figure 2.

As shown in the IS of Figure 2, CH_4 adsorbs on the Pd/In_2O_3(110) surface through a Pd−H bond with a distance of 1.87 Å, in contrast to the physisorption configuration on the CeO_2 and In_2O_3 surfaces.[14,15] The interaction of Pd with H resulted in a partial activation of the connecting C−H bond, as shown by the elongated C−H distance of 1.15 Å, from 1.09 Å of the gaseous CH_4 molecule. At the same time, the Pd−In_4 and Pd−O_5 bonds were broken and the Pd−O_2 bond was shortened from 2.16 to 2.02 Å. The Pd−In_2 bond distance remained almost at the same value, 2.61 Å. The adsorption energy of CH_4 was calculated to be −0.43 eV.

In the TS shown in Figure 2, the C−H bond was further stretched from 1.15 to 1.39 Å. The departing H atom moved toward the surface O_5 site, resulting in a H−O distance of 1.40 Å. Meanwhile, the distance of the carbon atom of CH_4 to the Pd site was reduced to 2.17 Å from 2.35 Å in the initial state. The Pd−C−H−O four-centered interaction resulted in facile activation of the C−H bond, with an activation barrier of only 0.39 eV. These results are consistent with the previous study of CH_4 activation on Pd and PdO clusters with different O coverages.[36] Chin and coauthors suggested that the heterolytic C−H bond dissociation on the Pd−O pair proceeded through a four-centered $(H_3C^{\delta-}\cdots Pd_{ox}\cdots H^{\delta+}\cdots O_{ox})^{\ddagger}$ transition state, resulting in a lower activation barrier than that on the O−O

https://doi.org/10.1021/acscatal.3c05163
ACS Catal. 2024, 14, 1714−1724

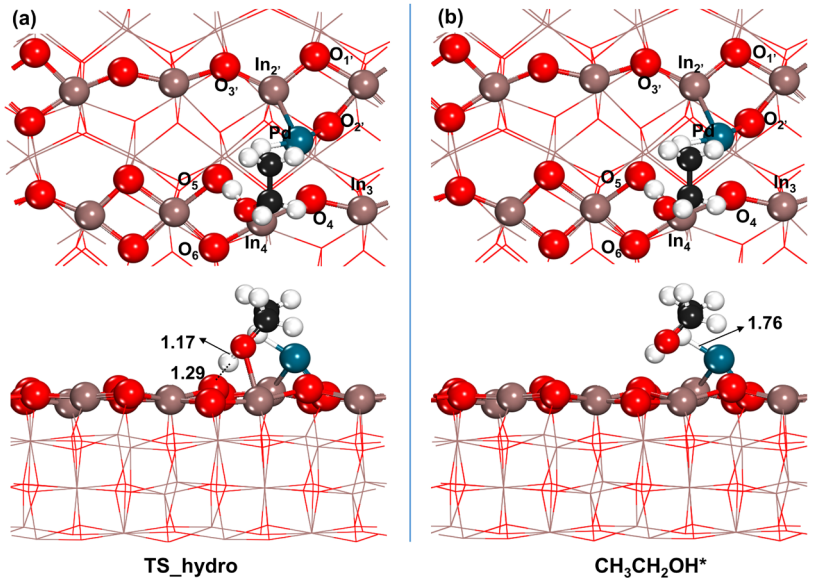

Figure 4. (a) Transition and (b) final states of ethoxy hydrogenation. Distances are in Å.

pair as the later involved formation of the radical-like CH_3 fragment prior to the formation of the C−O bond with the surface O atom. Following the C−H bond activation, the methyl species binds the Pd site with a Pd−C bond distance of 2.03 Å and the H atom occupies O_5, forming a H−O bond at a distance of 0.98 Å, as shown in FS of Figure 2. The overall reaction energy of this step was −0.33 eV.

We also considered CH_4 dissociation over the Pd−O_4, O_5−O_6, In_4−O_4, and In_4−O_5 pairs. The reaction energies were −0.34 eV, −0.31 eV, and 0.19 eV over the Pd−O_4, O_5−O_4, and In_4−O_5 pairs, respectively, referenced to the gaseous CH_4 molecule. Relaxation of the dissociated state over the In_4−O_4 pair resulted in the migration of CH_3* to vicinal Pd. Consequently, Pd−O remains the most active for CH_4 dissociation. We further tested the stability of the resulting CH_3 species on the Pd site by activating the C−H bond of the adsorbed CH_3 species with the assistance of the neighboring O_4 and $O_{2'}$ sites. Our results showed that this C−H bond activation step is endothermic by 0.62 and 0.41 eV on the O_4 and $O_{2'}$ sites, respectively, and therefore energetically unfavorable. Taking these results together, we conclude that the single Pd atom supported on the In_2O_3(110) surface promotes the first C−H bond activation of CH_4 while stabilizing the CH_3 species.

HCHO Adsorption and C−C Coupling Reaction. Starting from the coadsorbed CH_3 and H species, we introduced the HCHO molecule onto the surface of the catalyst. The optimized structures of HCHO adsorption, transition, and final states of C−C coupling are depicted in Figure 3.

To facilitate the C−C coupling reaction, we considered the In_4 site next to the adsorbed CH_3* species as the adsorption site for HCHO. The adsorption energy of HCHO at this site is −0.29 eV. As shown in Figure 3a, the HCHO molecule binds to the In_4 site through an In−O bond of 2.49 Å. The C−O bond was slightly elongated to 1.23 Å from 1.21 Å of the gas-phase molecule. To evaluate the impact of the activation sequence of CH_4 and HCHO on the coupling reaction, we considered the alternative pathway in which HCHO adsorbs on the Pd site first, followed by the dissociation of CH_4 on the In sites. The calculated adsorption energy of HCHO on the Pd site is −0.77 eV, comparable with the dissociative adsorption energy of CH_4 on the Pd site. However, the nearby In_4 site is endothermic by 0.19 eV and not active toward CH_4 dissociation. Additional microkinetic results shown in SI (Figure S4) indicate that the competitive adsorption of HCHO on the Pd sites will result in a decrease of the coverage of the intermediates from the C−C coupling steps and, thereby, the reaction. Nevertheless, the C−C coupling pathway remains operative, and the maximized reactivity can be achieved by dissociating CH_4 on the Pd site followed by adsorption of HCHO on the nearby In_4 site.

We tested the reactivity of HCHO direct oxidation by the vicinal O site on the In_2O_3 surface and found a reaction energy of 0.94 eV. These results indicate that In_2O_3 cannot oxidize HCHO, opening a possibility of In_2O_3 catalyzing the C−C coupling reaction.

On Pd/In_2O_3(110), the coupling of HCHO* with CH_3* follows a Langmuir−Hinshelwood mechanism. As an electrophile, the carbon center of HCHO* attacks the carbon center of the CH_3* species to form a C−C bond. In the transition state (Figure 3b), the C−O distance of HCHO was further extended to 1.28 Å. Meanwhile, HCHO was distorted from the coplanar structure, with a ∠H−CH−O dihedral angle of 151.3°. Consequently, the C atom was displaced toward the CH_3* species, resulting in an increased Pd−C distance of 2.14 Å. The C−C distance in the transition state is 2.19 Å. The activation barrier for coupling of CH_3* with HCHO* is 0.56 eV. This value is comparable to the activation barrier of gaseous CO_2 insertion into the M-CH_3* bond on the Zn-doped CeO_2 surface[14] but much lower than the coupling activation barrier of adsorbed CO_2* with M-CH_3* on the $(ZnO)_3$-supported In_2O_3 surface.[15] The results indicate that HCHO is a more potent electrophile than CO_2 in the coupling reaction with the CH_3* species. Moreover, this C−C coupling process has a lower activation barrier than that of the formation of the $CH_3CH_2OH^+$ complex from the collision of $HCHO^+$ with CH_4 (0.87 eV).[29] Therefore, Pd and In_2O_3 work synergistically toward C−C coupling of CH_3* with HCHO*.

https://doi.org/10.1021/acscatal.3c05163
ACS Catal. 2024, 14, 1714−1724

In the final state (Figure 3c), the newly formed C−C bond has a distance of 1.54 Å. The C−O distance increased to 1.39 Å from 1.28 Å at the transition state, indicating a conversion of the C−O double bond in the HCHO molecule to a C−O single bond. The formation of the C−C bond results in an adsorbed ethoxy species on the surface in a bidentate configuration, with O binding the surface In_4 atom and one H atom of the methyl group interacting with the Pd atom. The reaction energy of the C−C coupling step is −0.36 eV.

Formation of Ethanol. The resulting ethoxy species can react with the H adatom from CH_4 dissociation, producing ethanol. The optimized structures along the pathway of ethanol formation are given in Figure 4. In the transition state for ethoxy hydrogenation, the H adatom was displaced toward the O atom of the ethoxy species, reaching a O−H distance of 1.17 Å, while the H−O_5 distance was elongated to 1.29 Å, as shown in Figure 4a. This step overcomes a small activation barrier of 0.11 eV and has an overall reaction energy of 0.06 eV. The resulting ethanol adsorbs on the surface through a Pd−H bond, as shown in Figure 4b. The desorption of ethanol is endothermic by 0.64 eV.

Based on the above elementary steps, we mapped out the overall potential energy profile from gaseous CH_4 and HCHO to ethanol in Figure 5. The potential energy profile in Figure 5

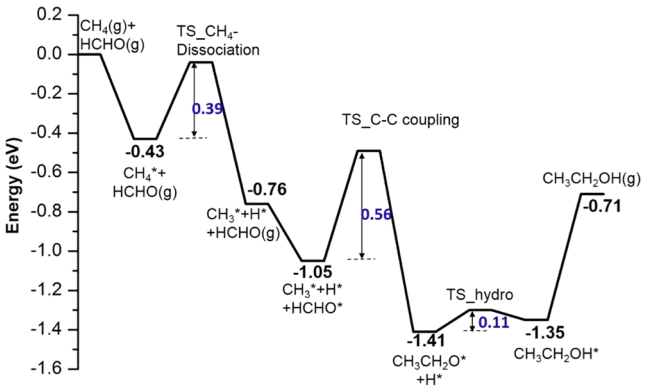

Figure 5. Potential energy profile of ethanol formation from CH_4 and HCHO. A* represents the adsorption state of A.

clearly shows that the formation of ethanol through C−C coupling of CH_4 with HCHO has an overall reaction energy of −0.71 eV and is thermodynamically favorable. We note that there has been a report of ethanol formation from CO insertion into the M-CH_3* bond in organometallics, followed by hydrogenation,[30] and formation of ethanol from CH_4 and HCHO has 100% atomic efficiency. In fact, HCHO has been believed to be an important intermediate in a heterogenous CO hydrogenation reaction.[31] Direct coupling of the CH_3* species with HCHO* through the surface-catalyzed C−C coupling to produce ethanol provides an alternative pathway for utilizing methane through an energy- and atom-efficient process.

Ethanol Formation on Other Single Metal Atoms on In_2O_3(110). So far, we have demonstrated that the activation of the first C−H bond in CH_4, C−C coupling, and ethoxy hydrogenation are key steps in ethanol formation from CH_4 and HCHO. We extended the study to other single metal atoms supported on the In_2O_3(110) surface to examine their performance for ethanol synthesis and develop an understanding of the underlying physicochemical origin of the activity. These atoms include the neighboring elements in the periodic table, i.e., Ni, Pt, Ag, and Rh. In each case, we studied the elementary steps for ethanol production from CH_4 and HCHO and tabulated the results of these steps, including CH_4 dissociation, the C−C coupling reaction, and ethoxy hydrogenation in Table 1. The relaxed structures of these steps on

Table 1. Activation Barriers and Reaction Energies of the CH_4 Dissociation, C−C Coupling Reaction, and Hydrogenation Reaction on Different Single Metal Atoms (Rh, Ni, Pd, Pt, Ag) on the In_2O_3(110) Surface

single atom	Rh	Ni	Pd	Pt	Ag
$\Delta E_{\_CH3*}$ (eV)	−0.21	−0.34	−0.33	−0.12	−0.40
$TS_{\_CH3*}$ (eV)	1.22	0.76	0.39	0.41	0.52
$\Delta E_{\_coup}$ (eV)	−0.17	0.15	−0.36	0.08	−0.95
$TS_{\_coup}$ (eV)	1.38	0.98	0.56	1.63	0.56
$\Delta E_{\_hydro}$ (eV)	−0.34	−0.6	0.06	−0.58	0.68
$TS_{\_hydro}$ (eV)	0.02	0.14	0.11	0.04	0.85

other single metal atoms supported on In_2O_3(110) are provided in the Supporting Information. Analysis of density of states was used to gain some insights into the interaction between the reaction intermediates and the active ensembles, as shown in Figure 6.

As shown in Table 1, Pd/In_2O_3 has the lowest activation barrier for the activation of the first C−H bond of CH_4. In contrast, the reaction on Ag/In_2O_3 is the most exothermic, attributable to a significant overlap between d-orbitals of Ag and s- and p-orbitals of C. The overlaps are at the lowest orbital energy, as shown in Figure 6a. The C−C coupling step on Ag/In_2O_3 has a reaction energy of −0.95 eV and is significantly exothermic, whereas this step on Ni/In_2O_3 and Pt/In_2O_3 becomes slightly endothermic. The resulting ethoxy species is bound to the surface through an In_4−O bond. The s- and p-orbitals of In_4 interact with the s- and p-orbitals of O of ethoxy at higher energy levels on Ni/In_2O_3 and Pt/In_2O_3, as depicted in Figure 6i,j, resulting in a weak interaction and thereby high coupling reaction energy. Although the C−C coupling step on Ni/In_2O_3 is the most endothermic, the hydrogenation step on Ni/In_2O_3 is the most exothermic. This is in accordance with the downward shift of the orbital overlap between In_4 and O of CH_3CH_2OH* on Ni/In_2O_3, as shown in Figure 6o. These results demonstrate that different single-metal atom catalysts affect each elementary step differently, and an optimal ethanol production is a result of balancing all the catalytic steps. A correlation of the three steps on different single metal atoms on In_2O_3(110) plotted in Figure 7 exemplifies such balance.

The blue line in Figure 7 clearly shows that there is a positive correlation between the dissociation energy of CH_4 and the C−C coupling energy, although Ni deviates from the trend line. This is consistent with the fact that Ni is an excellent catalyst for CH_4 dry reforming due to its extraordinary activity for CH_4 dissociation.[44] The red line in Figure 7 shows that the reaction energy of the ethoxy hydrogenation step correlates linearly and negatively with the C−C coupling energy. The C−C coupling step is the most exothermic on Ag/In_2O_3, but the hydrogenation step is the most endothermic. On Pt/In_2O_3 and Ni/In_2O_3, the hydrogenation step is favorable, but the CH_4 dissociation and C−C coupling steps are impeded. We note that the blue line crosses the red roughly at Pd, indicating that Pd offers a balanced

https://doi.org/10.1021/acscatal.3c05163
ACS Catal. 2024, 14, 1714−1724

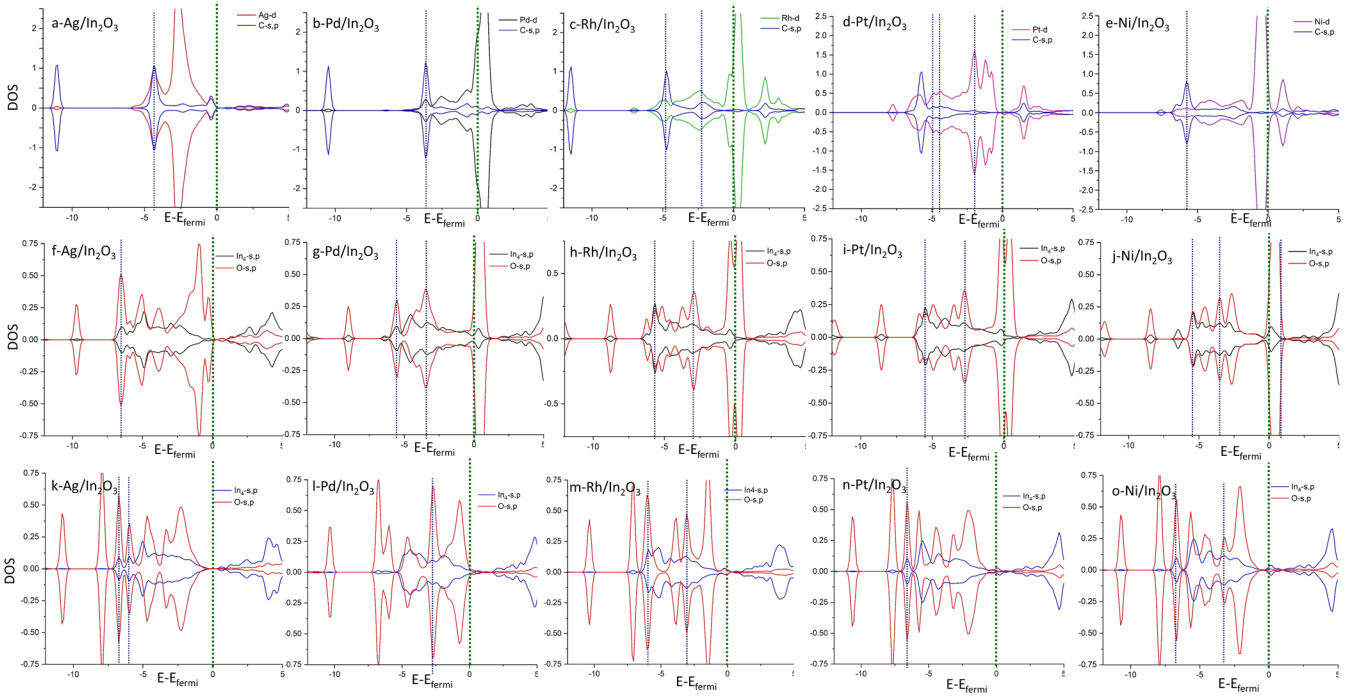

Figure 6. Density of states of the metal atom with the C center of CH_4*(a-e), In_4 with O of ethoxy species (f-j), and In_4 with O of CH_3CH_2OH* (k-o) on Ag/In_2O_3, Pd/In_2O_3, Rh/In_2O_3, Pt/In_2O_3, and Ni/In_2O_3.

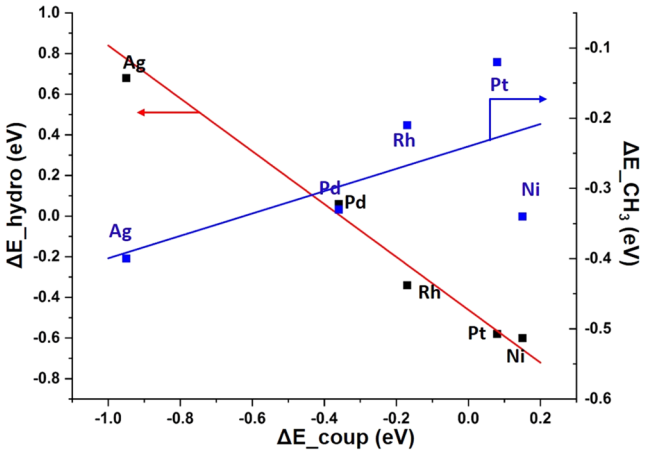

Figure 7. Correlations between the C−C coupling energy (ΔE_coup) and the ethoxy hydrogenation energy (ΔE_hydro) (left, red) and the CH_4 dissociation energy (right, ΔE_CH_3) (blue).

performance among the three key steps. Consequently, Pd/In_2O_3 is expected to provide optimal performance for ethanol production from CH_4 and HCHO.

Ethylene and Acetaldehyde Formation on $Pd/In_2O_3(110)$. As $Pd/In_2O_3(110)$ exhibits optimal performance for the reaction of CH_4 with HCHO to produce ethanol, we examined the possibility of forming other products on $Pd/In_2O_3(110)$. This was done by expanding the possible reaction pathways that the ethoxy species may undergo. These pathways include ethanol formation via hydrogenation, ethylene formation from dehydration, and acetaldehyde formation from dehydrogenation. The reaction pathway for ethanol formation on Pd/In_2O_3 has the advantage of achieving 100% atom efficiency and is discussed above. In what follows, we will present the results of ethylene and acetaldehyde formation.

Ethylene Formation. The corresponding structures along the pathway of ethylene formation from ethoxy species are depicted in Figure 8. As shown in Figure 8a, the departing H atom of the methyl group approaches the O site of the surface ethoxy species in the transition state. This H atom is stabilized by both C and O atoms, with a C−H distance of 1.42 Å and O−H distance of 1.31 Å. Meanwhile, the Pd−C distance was reduced to 2.28 Å, indicating a strengthening of the Pd−C interaction. In the final state, Figure 8b, the Pd−C bond was further shortened to 2.05 Å, and the H atom combined with the O site, forming a CH_2CH_2OH* species. The calculated activation barrier and reaction energy for the intramolecular H transfer step are 1.72 and −0.50 eV, respectively.

Following the intramolecular H transfer step, cleaving the C−OH bond will produce ethylene. The departing OH may combine with the H adatom from CH_4 dissociation to form a H_2O molecule. The activation barrier and reaction energy for the C−OH bond breaking step were calculated to be 0.81 and −0.32 eV, respectively. Following the breaking of the C−OH bond, the resulting ethylene species adsorbs on the Pd site in a π-mode with two equivalent Pd−C bonds at a distance of 2.12 Å. The adsorbed ethylene in this configuration is very stable, with the six atoms of ethylene being almost coplanar and a desorption energy of 1.2 eV. To complete the cycle, OH would combine with H to form H_2O. This step is endothermic by 0.50 eV and has an activation barrier of 0.57 eV. The desorption energy of water is 0.51 eV. The overall potential energy profile for ethylene production from CH_4 and HCHO is shown in Figure 9.

As shown in Figure 9, the overall reaction from CH_4 and HCHO to ethylene and water with a reaction energy of −0.02 eV is only slightly exothermic. Therefore, the formation of ethylene is less favorable than that of ethanol production (−0.71 eV). Furthermore, the high activation barrier for the H

https://doi.org/10.1021/acscatal.3c05163
ACS Catal. 2024, 14, 1714−1724

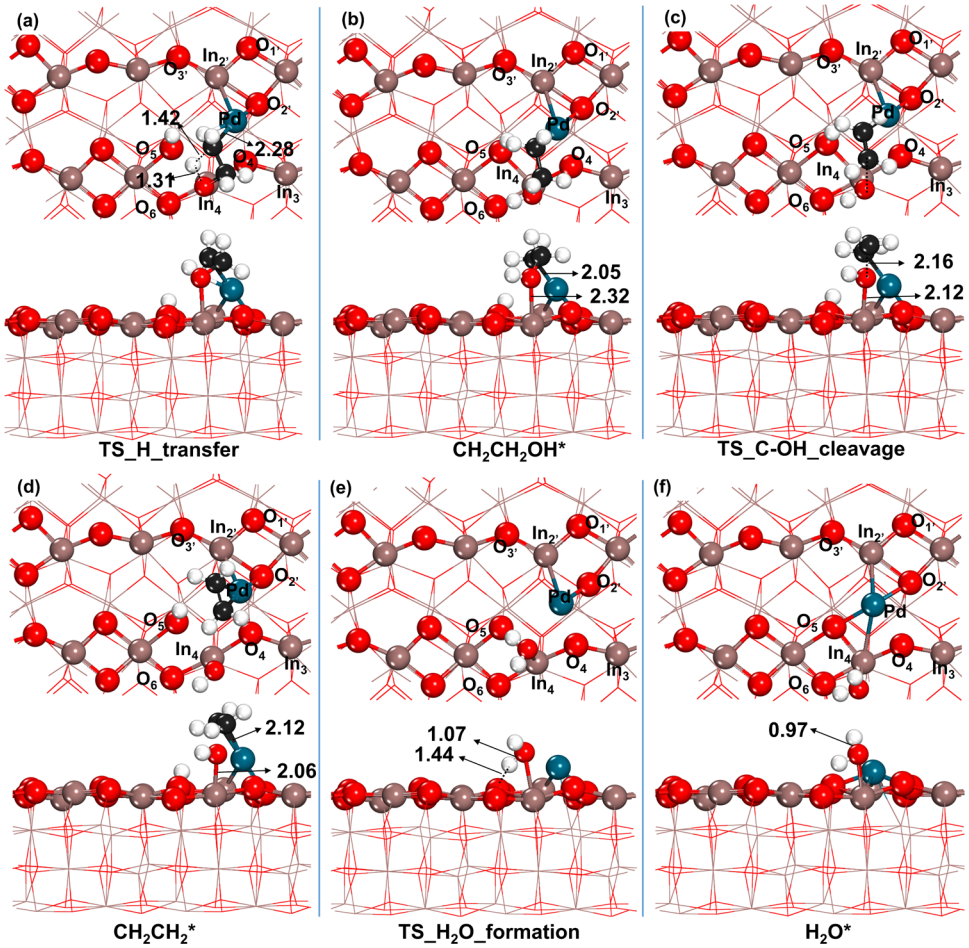

Figure 8. Optimized structures of transition states for (a) H transfer, (c) C−OH bond cleavage, and (e) H_2O formation and adsorbed intermediates including (b) CH_2CH_2OH, (d) CH_2CH_2, and (f) H_2O along the pathway of ethylene formation from the ethoxy species on Pd/In_2O_3(110). Distances are in Å.

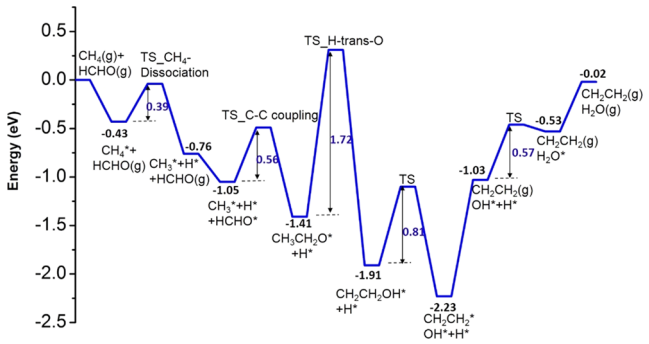

Figure 9. Potential energy profile of ethylene formation from CH_4 and HCHO on Pd/In_2O_3(110). A* represents the adsorption state of species A on the surface.

transfer step and the high desorption energy of the resulting ethylene would further impede the reaction along this pathway.

Acetaldehyde Formation. In addition to the production of ethanol and ethylene, dehydrogenation of the ethoxy species produces acetaldehyde. The process starts from dehydrogenation at the methylene end of the adsorbed ethoxy species, as shown in Figure 10a,b. One H of the methylene group tilts toward the surface O_4 site in the transition state of dehydrogenation. The C−H bond extends to 1.27 Å, while the H−O distance becomes 1.39 Å. The breaking of the C−H bond leads to the formation of an acetaldehyde species, which adsorbs on the surface through one Pd−C bond and one Pd−H bond. The cleavage of the C−H bond shortens the C−C distance from 1.52 to1.48 Å, while the C−O bond is reduced from 1.35 to1.23 Å. The calculated dehydrogenation activation barrier and reaction energy are 0.66 and −0.93 eV, respectively. These results indicate that production of the acetaldehyde species from the ethoxy species is thermodynamically favorable. The desorption energy of the acetaldehyde species is 0.71 eV. To complete the cycle, the remaining two H atoms on the surface would desorb as a H_2 molecule. The optimized structures along the pathway for H_2 formation are depicted in Figure 10c−f. The overall potential energy profile for the conversion of CH_4 and HCHO to acetaldehyde and H_2 is given in Figure 11.

We note that although the formation of acetaldehyde from the ethoxy species is both kinetically and thermodynamically possible, the final H_2 formation and desorption steps may prevent the reaction from proceeding through this pathway. According to the potential energy profile in Figure 11, the overall reaction from CH_4 and HCHO to acetaldehyde and H_2 is endothermic with a small reaction energy of 0.28 eV. However, the formation of acetaldehyde is thermodynamically the least favorable among ethanol, ethylene, and acetaldehyde. We further studied the selectivity toward the three possible

https://doi.org/10.1021/acscatal.3c05163
ACS Catal. 2024, 14, 1714−1724

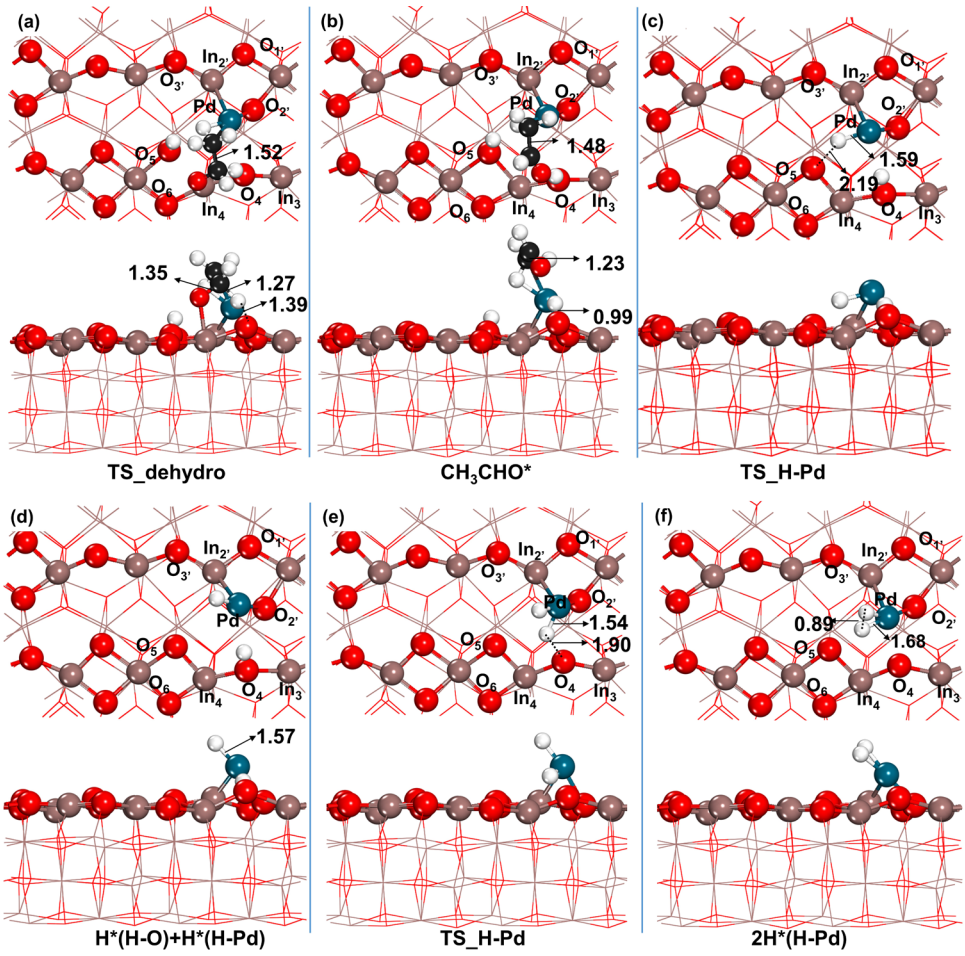

Figure 10. Optimized structures of transition states and intermediates along the pathway of acetaldehyde formation from the ethoxy species on Pd/In_2O_3(110). (a) Transition state for ethoxy dehydrogenation; (b) adsorbed acetaldehyde; (c) transition state for hydrogen transfer to Pd; (d) coadsorbed H atoms on Pd and O; (e) transition state for H transfer from O to Pd; and (f) two H atoms coadsorbed on Pd. Distances are in Å.

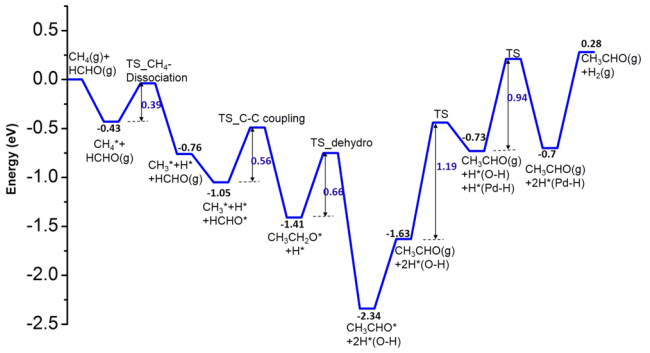

Figure 11. Potential energy profile for the conversion of CH_4 and HCHO to acetaldehyde and H_2 on Pd/In_2O_3(110). A* represents the adsorption state of species A on the surface.

products on Pd/In_2O_3(110) based on the microkinetic analysis.

Microkinetic Analysis. We performed a microkinetic analysis based on the DFT-calculated energetics, including reaction energies, activation barriers, and harmonic vibrational frequencies. To determine the selectivity, we included all elementary steps leading to the formation of ethanol, ethylene, and acetaldehyde. The forward and reverse rate constants of each elementary step as well as the corresponding equilibrium constant were calculated based on the transition state theory. The detailed equations are provided in the Supporting Information. The DFT results show that the three possible products share a common ethoxy species formed from the C−C coupling step. Therefore, the active sites for CH_4 and HCHO activation were not distinguished in the microkinetic modeling. Based on the elementary steps of the complete catalytic cycle on Pd/In_2O_3(110), a set of temporal differential equations for coverages of each intermediate can be written. Solving the set of differential equations numerically and normalizing the coverage of all surface species, we can obtain the coverage of each intermediate in the temperature range of 400−600 K. The dependence of surface coverage of CH_3CH_2OH*, CH_2CH_2*, and CH_3CHO* on temperature is shown in Figure 12a, where A* denotes the adsorbed state of species A on the surface. By calculating the reaction rate of the three products at the steady state, we determined selectivity and have shown them in Figure 12b.

As shown in Figure 12a, the steady-state surface coverage of ethanol increases as the temperature was raised, reaching ~0.8 at 500 K and is the dominant species below 550 K. This result is in consistency with the potential energy profiles in Figures 5, 9, and 11. The formation of CH_3CH_2OH* has the lowest activation barrier of 0.11 eV. The intramolecular hydrogen transfer step of the ethoxy species to form ethylene has the highest activation barrier of 1.72 eV, which is more sensitive to the increasing temperature. Increasing the temperature beyond

https://doi.org/10.1021/acscatal.3c05163
ACS Catal. 2024, 14, 1714−1724

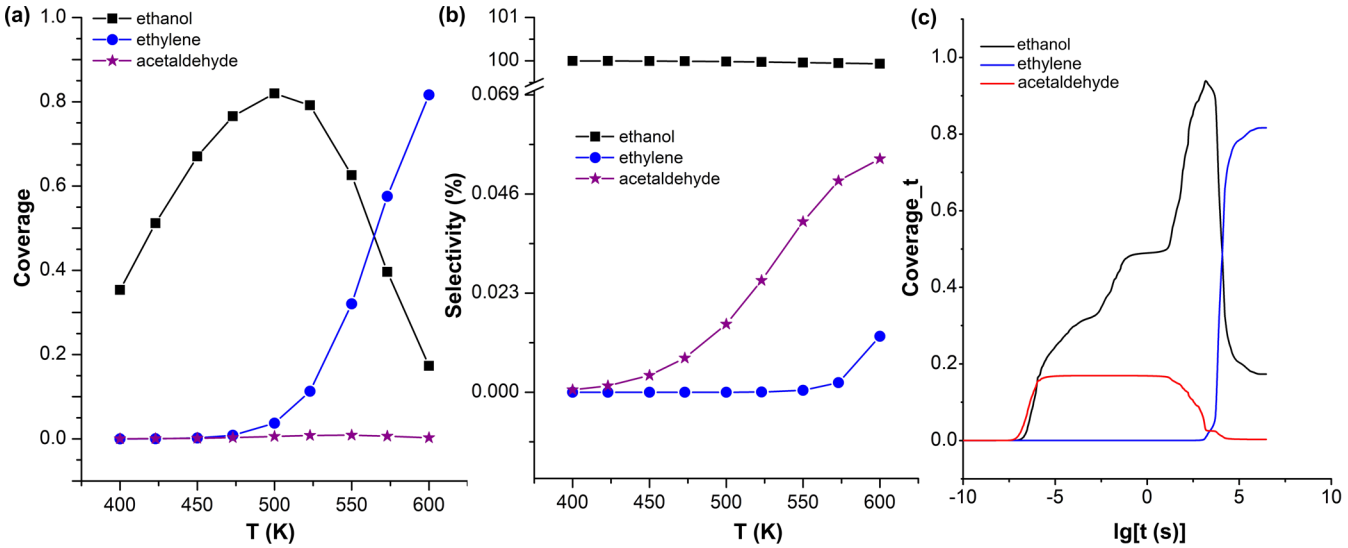

Figure 12. (a) Surface coverage and (b) selectivity of ethanol, ethylene, and acetaldehyde in the temperature range of 400−600 K and (c) temporal coverage of ethanol, ethylene, and acetaldehyde at 600 K.

550 K, CH_2CH_2* becomes the dominant species and has a coverage higher than that of CH_3CH_2OH*. However, the steady-state coverage of CH_3CHO* remains extremely low up to 600 K. As we mentioned before, the three possible products share the common CH_3CH_2O* species. The combination of CH_3CH_2O* with surface H* leads to the formation of CH_3CH_2OH*. If intramolecular hydrogen transfer occurred, i.e., $CH_3CH_2O^* \rightarrow CH_2CH_2OH^*$, followed by dropping the OH* group, CH_2CH_2* will be formed. However, the formation of CH_3CHO* needs an empty active site, i.e., $CH_3CH_2O^* + * \rightarrow CH_3CHO^* + H^*$. As shown by the temporal distribution of surface coverages at 600 K in Figure 12c, the surface is covered primarily by CH_3CH_2OH* at the initial stage of the reaction and the coverage of CH_3CHO* rises to ∼0.16, whereas the coverage of CH_2CH_2* remains extremely low. However, as acetaldehyde is formed and H* accumulates on the surface. Desorption of H* as H_2 needs to overcome a barrier of 1.19 eV for H transfer and a reaction energy of 1.26 eV for H_2 formation. This highly endothermic step, together with the high desorption energy of 0.71 eV for acetaldehyde and 1.20 eV for ethylene, hindered the regeneration of active sites. As a result, the $CH_3CH_2O^* + * \rightarrow CH_3CHO^*$ step leads to a decrease of the CH_3CHO* coverage. At the same time, the remaining H* will likely combine with surface OH* to form H_2O*, which in return facilitates the C−OH* cleavage of CH_2CH_2OH* to form ethylene, as shown in Figure 12c.

The selectivity toward each product is shown in Figure 12b. Clearly, ethanol is the main product, with a selectivity of >99.9%, and the combined selectivity for ethylene and acetaldehyde is under 0.1% in a temperature range of 400−600 K. The observed selectivity correlates with the surface coverages of CH_3CH_2OH*, CH_2CH_2*, and CH_3CHO* and reflects the fact that the desorption energy of ethanol is 0.64 eV, lower than that of ethylene (1.20 eV) and acetaldehyde (0.71 eV). Moreover, along the ethylene and acetaldehyde formation pathways, additional steps are needed. Increasing the reaction temperature would enhance the selectivity toward both ethylene and acetaldehyde. At 600 K, a sharp increase in the selectivity of ethylene can be observed although the selectivity is still very low (<0.1%). The selectivity toward acetaldehyde also shows an increase but remains to be less than 0.1%. As such, ethanol is the dominant product of the single-atom $Pd/In_2O_3(110)$ catalyst. More comprehensive analysis may change some details of the results but is not expected to affect the qualitative conclusion. The microkinetic analysis based on the DFT results confirmed an atom-economic ethanol formation with high selectivity on the single Pd atom supported-on-In_2O_3 catalyst.

CONCLUSIONS

A single-atom Pd/In_2O_3 (110) catalyst was demonstrated to catalyze the C−C coupling reaction of CH_4 with HCHO. The Pd site facilitates CH_4 adsorption through the formation of a Pd−H bond. Breaking the first C−H bond of CH_4 on the Pd site is thermodynamically and kinetically favorable, resulting in the formation of the Pd-CH_3* species. The adsorbed HCHO on the In site can couple with the CH_3* species on the Pd site to form the ethoxy species, which will subsequently combine with H* to produce ethanol. The formation of ethanol from CH_4 and HCHO has 100% atom efficiency. Examining other single metal atoms, including Ni, Rh, Pt, and Ag, on In_2O_3 (110) as the active center for the same reactions showed that Pd/In_2O_3 (110) offers a balanced reactivity toward CH_4 dissociation, C−C coupling, and ethoxy species hydrogenation and is the optimal catalyst for ethanol formation. Microkinetic analysis was used to integrate the DFT results and compare the productions of ethanol, ethylene, and acetaldehyde on $Pd/In_2O_3(110)$. The results showed that ethanol is the dominant product with a selectivity of >99.9% in the temperature range of 400−600 K. These findings predict that the single-atom Pd/In_2O_3 catalyst selectively catalyzes the C−C coupling of CH_4 and HCHO to produce ethanol and offer new ideas of designing novel catalysts for natural gas utilization and catalytic removal of HCHO.

ASSOCIATED CONTENT

Supporting Information

The Supporting Information is available free of charge on the ACS Publications website. The Supporting Information is available free of charge at https://pubs.acs.org/doi/10.1021/acscatal.3c05163.

https://doi.org/10.1021/acscatal.3c05163
ACS Catal. 2024, 14, 1714−1724

Structures of single Pd atom supported on the $In_2O_3(110)$ surface, microkinetic analysis, and structures of Ni, Pt, Ag, and Rh supported on the $In_2O_3(110)$ surface (PDF)

AUTHOR INFORMATION

Corresponding Authors

Xinli Zhu − *Collaborative Innovation Center of Chemical Science and Engineering, School of Chemical Engineering and Technology, Tianjin University, Tianjin 300072, China;* orcid.org/0000-0002-8681-9994; Email: xinlizhu@tju.edu.cn

Qingfeng Ge − *Department of Chemistry and Biochemistry, Southern Illinois University, Carbondale, Illinois 62901, United States;* orcid.org/0000-0001-6026-6693; Email: qge@chem.siu.edu

Authors

Yuntao Zhao − *School of Materials and Chemical Engineering, Ningbo University of Technology, Ningbo 315211, China; Collaborative Innovation Center of Chemical Science and Engineering, School of Chemical Engineering and Technology, Tianjin University, Tianjin 300072, China; Department of Chemistry and Biochemistry, Southern Illinois University, Carbondale, Illinois 62901, United States*

Natalie Fontillas − *Department of Chemistry and Biochemistry, Southern Illinois University, Carbondale, Illinois 62901, United States*

Hua Wang − *Collaborative Innovation Center of Chemical Science and Engineering, School of Chemical Engineering and Technology, Tianjin University, Tianjin 300072, China;* orcid.org/0000-0002-8305-3655

Donghai Mei − *Institute for Integrated Catalysis, Pacific Northwest National Laboratory, Richland, Washington 99352, United States; State Key National Laboratory of Membrane Separation and Membrane Processes, School of Chemistry and Chemical Engineering, Tianjin Polytechnic University, Tianjin 300387, China;* orcid.org/0000-0002-0286-4182

Complete contact information is available at: https://pubs.acs.org/10.1021/acscatal.3c05163

Notes

The authors declare no competing financial interest.

ACKNOWLEDGMENTS

The authors acknowledge the financial support of the National Natural Science Foundation of China (Grants 22103044, 21676194 and 21873067). Y.Z. thanks the joint Ph.D. scholarship support from the China Scholarship Council. The computations were supported partly by the scientific theme user proposal in the William R. Wiley Environmental Molecular Sciences Laboratory (EMSL), which is a US Department of Energy national scientific user facility located at PNNL in Richland, Washington. Q.G. acknowledges the support of the NSF-CBET program (Award CBET-1438440).

REFERENCES

(1) Gao, W.; Liang, S.; Wang, R.; Jiang, Q.; Zhang, Y.; Zheng, Q.; Xie, B.; Toe, C. Y.; Zhu, X.; Wang, J. Industrial Carbon Dioxide Capture and Utilization: State of the Art and Future Challenges. *Chem. Soc. Rev.* **2020**, *49*, 8584−8686, DOI: 10.1039/d0cs00025f.

(2) Fletcher, S. E. M.; Schaefer, H. Rising Methane: A New Climate Challenge. *Science* **2019**, *364*, 932−933.

(3) Chen, L.; Msigwa, G.; Yang, M.; Osman, A. I.; Fawzy, S.; Rooney, D. W.; Yap, P. S. Strategies to Achieve a Carbon Neutral Society: A Review. *Environ. Chem. Lett.* **2022**, *20*, 2277−2310.

(4) Pekkarinen, V. Going Beyond Co_2: Strengthening Action on Global Methane Emissions under the UN Climate Regime. *Rev. Eur., Comp. Int. Environ. Law* **2020**, *29*, 464−478.

(5) Nzotungicimpaye, C.-M.; MacIsaac, A. J.; Zickfeld, K. Delaying Methane Mitigation Increases the Risk of Breaching the 2 °C Warming Limit. *Commun. Earth Environ.* **2023**, *4*, No. 250, DOI: 10.21203/rs.3.rs-1823460/v1.

(6) Mar, K. A.; Unger, C.; Walderdorff, L.; Butler, T. Beyond CO_2 Equivalence: The Impacts of Methane on Climate, Ecosystems, and Health. *Environ. Sci. Policy.* **2022**, *134*, 127−136.

(7) Rocher-Ros, G.; Stanley, E. H.; Loken, L. C.; Casson, N. J.; Raymond, P. A.; Liu, S.; Amatulli, G.; Sponseller, R. A. Global Methane Emissions from Rivers and Streams. *Nature* **2023**, *621*, 530.

(8) Hutchings, G. J.; Scurrell, M. S.; Woodhouse, J. R. Oxidative Coupling of Methane Using Oxide Catalysts. *Chem. Soc. Rev.* **1989**, *18*, 251−283.

(9) Lunsford, J. H. The Catalytic Oxidative Coupling of Methane. *Angew. Chem., Int. Ed.* **1995**, *34*, 970−980.

(10) Periana, R. A.; Mironov, O.; Taube, D.; Bhalla, G.; Jones, C. J. Catalytic, Oxidative Condensation of CH_4 to CH_3COOH in One Step Via CH Activation. *Science* **2003**, *301*, 814−818.

(11) Periana, R. A.; Taube, D. J.; Gamble, S.; Taube, H.; Satoh, T.; Fujii, H. Platinum Catalysts for the High-Yield Oxidation of Methane to a Methanol Derivative. *Science* **1998**, *280*, 560−564.

(12) Stoppioni, P.; Dapporto, P.; Sacconi, L. Insertion Reaction of Carbon Monoxide into Metal-Carbon Bonds. Synthesis and Structural Characterization of Cobalt(II) and Nickel(II) Acyl Complexes with Tri(Tertiary Arsines and Phosphines). *Inorg. Chem.* **1978**, *17*, 718−725.

(13) Stavropoulos, P.; Muetterties, M. C.; Carrie, M.; Holm, R. H. Structural and Reaction Chemistry of Nickel Complexes in Relation to Carbon Monoxide Dehydrogenase: A Reaction System Simulating Acetyl-Coenzyme a Synthase Activity. *J. Am. Chem. Soc.* **1991**, *113*, 8485−8492.

(14) Zhao, Y.; Cui, C.; Han, J.; Wang, H.; Zhu, X.; Ge, Q. Direct C-C Coupling of CO_2 and the Methyl Group from CH_4 Activation through Facile Insertion of CO_2 into Zn-Ch_3 σ-Bond. *J. Am. Chem. Soc.* **2016**, *138*, 10191−10198.

(15) Zhao, Y.; Wang, H.; Han, J.; Zhu, X.; Mei, D.; Ge, Q. Simultaneous Activation of CH_4 and CO_2 for Concerted C−C Coupling at Oxide−Oxide Interfaces. *ACS Catal.* **2019**, *9*, 3187−3197.

(16) Salthammer, T.; Mentese, S.; Marutzky, R. Formaldehyde in the Indoor Environment. *Chem. Rev.* **2010**, *110*, 2536−2572.

(17) Kerns, W. D.; Pavkov, K. L.; Donofrio, D. J.; Gralla, E. J.; Swenberg, J. A. Carcinogenicity of Formaldehyde in Rats and Mice after Long-Term Inhalation Exposure. *Cancer Res.* **1983**, *43*, 4382−4392.

(18) Domingo-García, M.; Fernández-Morales, I.; López-Garzón, F. J.; Moreno-Castilla, C.; Pérez-Mendoza, M. On the Adsorption of Formaldehyde at High Temperatures and Zero Surface Coverage. *Langmuir* **1999**, *15*, 3226−3231.

(19) Wang, H.; Zhao, X.; Huang, C.; Jin, X.; Wei, D.; Dai, D.; Ma, Z.; Li, W. X.; Yang, X. Adsorption Features of Formaldehyde on $TiO_2(110)$ Surface Probed by High-Resolution Scanning Tunnelling Microscopy. *J. Phys. Chem. Lett.* **2019**, *10*, 3352−3358.

(20) Liu, Z.; Niu, J.; Long, W.; Cui, B.; Song, K.; Dong, F.; Xu, D. Highly Efficient MnO_2/AlOOH Composite Catalyst for Indoor Low-Concentration Formaldehyde Removal at Room Temperature. *Inorg. Chem.* **2020**, *59*, 7335−7343.

(21) Robert, B.; Nallathambi, G. Indoor Formaldehyde Removal by Catalytic Oxidation, Adsorption and Nanofibrous Membranes: A Review. *Environ. Chem. Lett.*. **2021**, *19*, 2551−2579.

(22) Wang, H.; Huang, Z.; Jiang, Z.; Jiang, Z.; Zhang, Y.; Zhang, Z.; Shangguan, W. Trifunctional C@MnO Catalyst for Enhanced Stable Simultaneously Catalytic Removal of Formaldehyde and Ozone. *ACS Catal.* **2018**, *8*, 3164−3180.
(23) Chen, D.; Zhang, G.; Wang, M.; Li, N.; Xu, Q.; Li, H.; He, J.; Lu, J. Pt/MnO_2 Nanoflowers Anchored to Boron Nitride Aerogels for Highly Efficient Enrichment and Catalytic Oxidation of Formaldehyde at Room Temperature. *Angew. Chem., Int. Ed.* **2021**, *60*, 6377−6381.
(24) Jin, Z.; Wang, L.; Hu, Q.; Zhang, L.; Xu, S.; Dong, X.; Gao, X.; Ma, R.; Meng, X.; Xiao, F.-S. Hydrophobic Zeolite Containing Titania Particles as Wettability-Selective Catalyst for Formaldehyde Removal. *ACS Catal.* **2018**, *8*, 5250−5254.
(25) Chen, M.; Wang, W.; Qiu, Y.; Wen, H.; Li, G.; Yang, Z.; Wang, P. Identification of Active Sites in HCHO Oxidation over TiO_2-Supported Pt Catalysts. *ACS Catal.* **2022**, *12*, 5565−5573.
(26) Liu, J.; Uselman, B.; Van Devener, B.; Anderson, S. L. Vibrational Mode Effects as a Probe of Inter-Channel Coupling in the Reactions of Formaldehyde Cation with Ammonia and Water†. *J. Phys. Chem. A* **2004**, *108*, 9945−9956.
(27) Van de Vyver, S.; Odermatt, C.; Romero, K.; Prasomsri, T.; Román-Leshkov, Y. Solid Lewis Acids Catalyze the Carbon−Carbon Coupling between Carbohydrates and Formaldehyde. *ACS Catal.* **2015**, *5*, 972−977.
(28) Wang, S.; Iglesia, E. Entropy-Driven High Reactivity of Formaldehyde in Nucleophilic Attack by Enolates on Oxide Surfaces. *J. Am. Chem. Soc.* **2018**, *140*, 775−782.
(29) Liu, J.; Van Devener, B.; Anderson, S. L. Reaction of Formaldehyde Cation with Methane: Effects of Collision Energy and H_2CO^+ and Methane Vibrations. *J. Chem. Phys.* **2003**, *119*, 200−214.
(30) Zhang, A.; Raje, S.; Liu, J.; Li, X.; Angamuthu, R.; Tung, C.-H.; Wang, W. Nickel-Mediated Stepwise Transformation of CO to Acetaldehyde and Ethanol. *Organometallics* **2017**, *36*, 3135−3141.
(31) Remediakis, I. N.; Abild-Pedersen, F.; Nørskov, J. K. DFT Study of Formaldehyde and Methanol Synthesis from CO and H_2 on Ni(111)†. *J. Phys. Chem. B* **2004**, *108*, 14535−14540.
(32) Ban, T.; Yu, X.-Y.; Tian, H.-K.; Huang, Z.-Q.; Chang, C.-R. One-step Conversion of Methane and Formaldehyde to Ethanol over SA-FLP Dual-Active-Site Catalysts: A DFT Study. *Chin. Chem. Lett.* **2023**, No. 108549.
(33) Wang, A.; Li, J.; Zhang, T. Heterogeneous Single-Atom Catalysis. *Nat. Rev. Chem.* **2018**, *2*, 65−81.
(34) Li, J.; Stephanopoulos, M. F.; Xia, Y. Introduction: Heterogeneous Single-Atom Catalysis. *Chem. Rev.* **2020**, *120*, 11699−11702.
(35) Zhang, X.; Sun, Z.; Wang, B.; Tang, Y.; Nguyen, L.; Li, Y.; Tao, F. F. C-C Coupling on Single-Atom-Based Heterogeneous Catalyst. *J. Am. Chem. Soc.* **2018**, *140*, 954−962.
(36) Chin, Y. H.; Buda, C.; Neurock, M.; Iglesia, E. Consequences of Metal-Oxide Interconversion for C-H Bond Activation During CH_4 Reactions on Pd Catalysts. *J. Am. Chem. Soc.* **2013**, *135*, 15425−15442.
(37) Su, Y. Q.; Filot, I. A. W.; Liu, J. X.; Hensen, E. J. M. Stable Pd-Doped Ceria Structures for CH_4 Activation and CO Oxidation. *ACS Catal.* **2018**, *8*, 75−80.
(38) Kresse, G.; Hafner, J. Ab Initio Molecular Dynamics for Open-Shell Transition Metals. *Phys. Rev. B* **1993**, *48*, 13115−13118.
(39) Kresse, G.; Furthmüller, J. Efficient Iterative Schemes for Ab Initio Total-Energy Calculations Using a Plane-Wave Basis Set. *Phys. Rev. B* **1996**, *54*, 11169−11186.
(40) Perdew, J. P.; Burke, K.; Ernzerhof, M. Generalized Gradient Approximation Made Simple. *Phys. Rev. Lett.* **1996**, *77*, 3865−3868.
(41) Kresse, G.; Joubert, D. From Ultrasoft Pseudopotentials to the Projector Augmented-Wave Method. *Phys. Rev. B* **1999**, *59*, 1758−1775.
(42) Blöchl, P. E. Projector Augmented-Wave Method. *Phys. Rev. B* **1994**, *50*, 17953−17979.
(43) Walsh, A.; Catlow, C. R. A. Structure, Stability and Work Functions of the Low Index Surfaces of Pure Indium Oxide and Sn-Doped Indium Oxide (ITO) from Density Functional Theory. *J. Mater. Chem.* **2010**, *20*, 10438−10444.
(44) Huang, J.; Liu, W.; Yang, Y.; Liu, B. High-Performance Ni−Fe Redox Catalysts for Selective CH_4 to Syngas Conversion via Chemical Looping. *ACS Catal.* **2018**, *8*, 1748−1756.

https://doi.org/10.1021/acscatal.3c05163
ACS Catal. 2024, 14, 1714−1724